SPATIO-TEMPORAL TURBULENT STRUCTURES OF THERMAL BOUNDARY LAYER SUBJECTED TO NON-EQUILIBRIUM ADVERSE PRESSURE GRADIENT

T. Houra
Department of Environmental Technology,
Nagoya Institute of Technology
Gokiso-cho, Showa-ku, Nagoya 466-8555, Japan
houra@heat.mech.nitech.ac.jp

S. Shakouchi and Y. Nagano
Department of Mechanical Engineering,
Nagoya Institute of Technology
Gokiso-cho, Showa-ku, Nagoya 466-8555, Japan
nagano@heat.mech.nitech.ac.jp

ABSTRACT

We have experimentally investigated a non-equilibrium turbulent boundary layer subjected to an adverse-pressure-gradient developing on a uniformly heated flat wall. The spatio-temporal structures educed from a multi-point simultaneous measurement are reasonably interpolated based on the "proper orthogonal decomposition (POD)". In the near-wall region, elongated hot regions stay dull and less active; on the other hand, large-scale cold regions having strong energy frequently invade the near-wall region. Then, the energy-containing events in the near-wall region are discussed based on the results of wavelet analysis.

INTRODUCTION

Characteristics of turbulent boundary-layer flows with adverse pressure gradients (APG) differ significantly from those of canonical boundary layers (Bradshaw, 1967; Spalart and Watmuff, 1993; Krogstad and Skåre, 1995). With respect to the heat transfer characteristics in APG boundary layers, classical experimental data under an equilibrium APG condition (Blackwell *et al.*, 1972) are used in order to validate proposed turbulence models and/or theory (Huang and Bradshaw, 1995; Volino and Simon, 1997). Actual flow fields, however, are usually encountered in a more complex situation, such as non-equilibrium pressure gradients. Thus, in order to improve the model predictions for practical usage, we must elucidate non-equilibrium APG effects on turbulent boundary layers with heat transfer.

From our previous heat transfer experiment on a non-equilibrium APG turbulent boundary layer (Houra and Nagano, 2006), we obtained the following results: (1) the standard log-law for both velocity and temperature profiles in a zero-pressure-gradient (ZPG) boundary layer does not hold in APG boundary layers; (2) the Stanton number follows the correlation curve for ZPG flows, although the corresponding skin friction coefficient decreases drastically; and (3) both the ejection and sweep-motions contribute significantly to the heat transport in APG flows, though sweep motions with shorter durations are the main contributor to the momentum transfer.

In this paper, multi-point simultaneous measurements of velocity and thermal fields are introduced to investigate the effect of the non-equilibrium APG on the interaction between large-scale motions in the outer layer and small-scale coherent structures near the wall. An array of five identical three-wire probes, each composed of an X-wire and a fine cold wire, is aligned in the wall-normal direction to measure simultaneously the velocity and thermal fields. From the measured velocity components in the streamwise and wall-normal directions and relevant temperature, the turbulent heat transfer field can be interpolated using the "proper orthogonal decomposition (POD)" for spatially interpolating the data. Then, the energy-containing events in the near-wall region are discussed based on the results of wavelet analysis.

EXPERIMENTAL APPARATUS

The experimental apparatus used is the same as described in our previous studies (Nagano *et al.*, 1998; Houra *et al.*, 2000; Houra and Nagano, 2006). For the heat transfer experiment, a flat plate, on which an air-flow turbulent boundary layer develops, is constructed with the 2-mm thick copper plate and a.c. heated from the back of the plate. The wall temperature distribution is monitored through embedded thermocouples and kept uniform during the experiment. The test section is composed of the heated flat-plate and a roof-plate to adjust pressure gradients (see Nagano *et al.*, 1998). The aspect ratio at the inlet to the test section is 13.8 (50.7 mm high × 700 mm wide). Under the present measurement conditions, the free-stream turbulence level is below 0.1%. To generate a stable turbulent boundary layer, a row of equilateral triangle plates is located at the inlet to the test section as a tripping device. The important flow parameters are listed in Table 1. In the APG flow, the pressure gradient dCp/dx keeps a nearly constant value of 0.6 m^{-1} over the region 65 mm $\leq x \leq$ 700 mm, and then decreases slowly (x is the streamwise distance from a tripping point). The pressure gradient parameter normalized by in-

Table 1: Flow parameters ($\overline{U}_0$=10.8 m/s, $\Delta\overline{\Theta}_e$= 10 K)

x [mm]	$\overline{U}_e$ [m/s]	δ [mm]	Δ [mm]	R_{δ_2}	R_{Δ_2}	P^+ $\times 10^2$	β
935 (ZPG)	10.8	19.9	21.0	1620	1920	0	0
535 (APG)	9.1	16.2	19.4	1330	1160	0.91	0.77
735 (APG)	8.3	24.6	25.3	1930	1280	1.93	2.19
935 (APG)	7.6	34.2	37.1	2730	1730	2.56	3.95

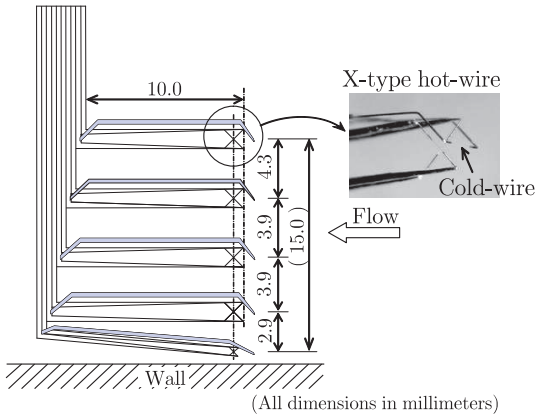

Figure 1: Array of five X-I probes for multi-point simultaneous measurement.

ner variables P^+ and the Clauser parameter β increase with increasing x, thus yielding moderate to strong APG.

Velocity and temperature fluctuations were simultaneously measured by the specially devised hot- and cold-wire technique. The probe consisted of three fine wires: the upstream wire serving as the constant current cold-wire (platinum 90%/ rhodium 10%; diameter 0.625 μm; length 1.0 mm $\simeq$ 18 in wall units; length-to-diameter ratio is 1600), and the two symmetrically-bent V-shaped hot-wires (Hishida and Nagano, 1988a, 1988b; tungsten; diameter 5 μm; length 0.8 mm). An array of five identical three-wire probes, each composed of an X-wire and a fine cold wire, is aligned in the wall-normal direction for simultaneous measurement, as shown in Fig. 1. The shape of this array is designed to measure the velocity and thermal fields simultaneously, where the effects of APG become significant, i.e., the buffer region: $y^+ = 20.7$ ($y/\delta \simeq 0.04$), two locations in the log region: $y^+ = 68.3$ ($y/\delta \simeq 0.12$), $y^+ = 131.6$ ($y/\delta \simeq 0.24$), the outer edge of the log region: $y^+ = 192.6$ ($y/\delta \simeq 0.35$), and the outer layer: $y^+ = 263.0$ ($y/\delta \simeq 0.48$). The two velocity components in the streamwise and wall-normal directions and temperature are measured simultaneously, and a set of these data at different y values from the measurement points are interpolated using the proper orthogonal decomposition (Houra *et al.*, 2000).

RESULTS AND DISCUSSION

Statistical characteristics and waveforms

Figure 2 shows the mean velocity profiles normalized by the free-stream velocity $\overline{U}/\overline{U}_e$. With increasing P^+, the defect in the mean velocity $\overline{U}$ from the free-stream velocity $\overline{U}_e$ becomes larger. Thus, in the outer coordinates, the mean velocity profile does not maintain self-similarity under the non-equilibrium condition. Figure 3 shows the mean temperature profiles normalized by the temperature difference between the wall and the ambient, $\overline{\Theta}/\overline{\Theta}_e$ [$= (\overline{T}_w - \overline{T})/(\overline{T}_w - \overline{T}_e)$]. The abscissa is the distance from the wall normalized by the 99% thickness of the thermal boundary layer. As clearly seen from this figure, there are few effects of APG on the mean temperature profiles on the basis of this normalization (Houra and Nagano, 2006).

Figure 4 shows the profiles of Reynolds shear stress, $-\overline{uv}$, normalized by the friction velocity, u_τ. The abscissa is the distance from the wall normalized by the 99% thickness of the boundary layer, δ. It includes the experimental and

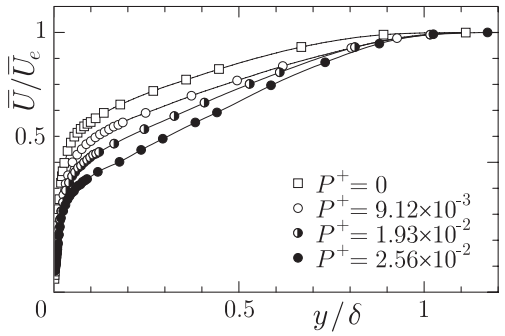

Figure 2: Mean velocity profiles in ZPG and APG flows in outer coordinates.

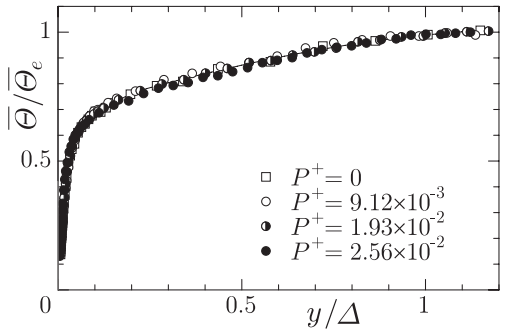

Figure 3: Mean temperature profiles in ZPG and APG flows in outer coordinates.

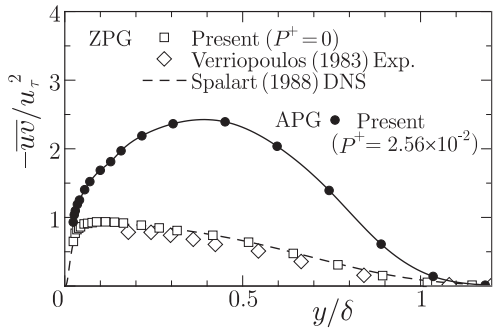

Figure 4: Reynolds shear stress in ZPG and APG flows.

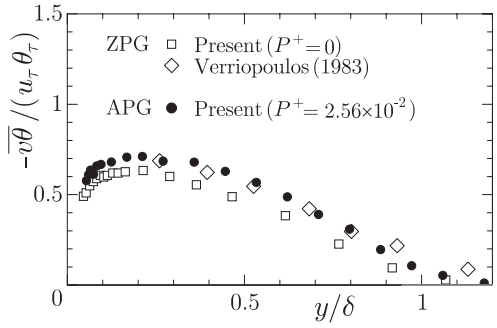

Figure 5: Wall-normal turbulent heat flux in ZPG and APG flows.

numerical results in ZPG flows (Verriopoulos, 1983; Spalart, 1988). With increasing P^+, $-\overline{uv}/u_\tau^2$ drastically increases in the outer region. Thus, the constant-stress layer relationship $-\overline{uv}/u_\tau^2 \simeq 1$ observed in the ZPG flows is no longer valid. This, too, may account for the non-existence of the universal law of the wall in APG boundary layers (not shown here). Figure 5 shows the wall-normal heat flux, $-\overline{v\theta}$, normalized

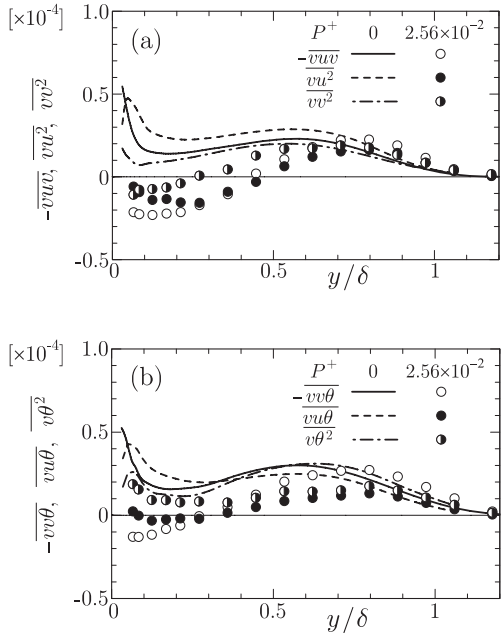

Figure 6: Distributions of turbulent transport in ZPG and APG flows: (a) velocity field; (b) thermal field. Velocity and temperature fluctuations are normalized by $\overline{U}_0$ and $\overline{\Theta}_e$, respectively.

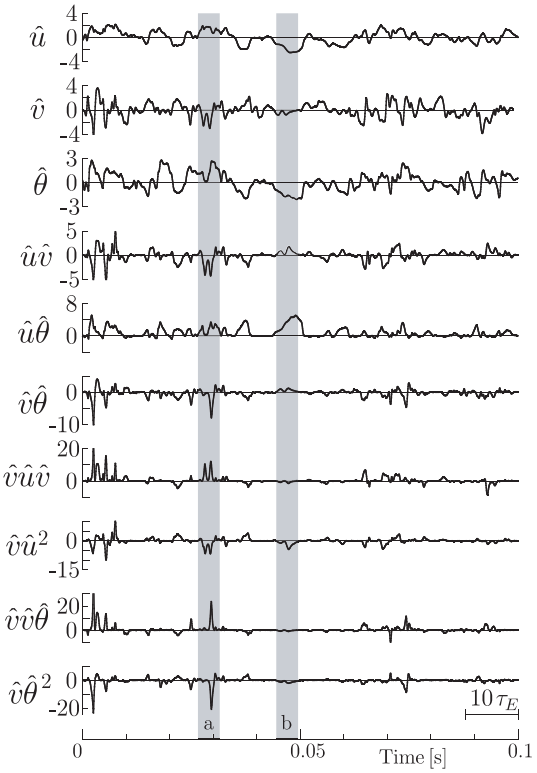

Figure 7: Velocities and temperature signal traces in APG flow ($y^+ = 20.7$, $y/\delta = 0.04$).

by the friction velocity, u_τ, and temperature, θ_τ, in ZPG and APG flows. The fluctuating temperature difference, θ, is defined as $\theta = \Theta - \overline{\Theta} = \overline{T} - T$. Thus, $\theta < 0$ indicates hotter than the mean temperature, and $\theta > 0$ colder.

As seen from Fig. 5, the wall-normal heat flux in APG flow is kept unchanged over the entire region compared with Reynolds shear stress in Fig. 4. In our previous experiment (Nagano *et al.*, 1998), the intensity of the wall-normal velocity component, v, normalized by freestream velocity, $\overline{U}_0$, at the inlet to the test section, was not affected. Because the heat transfer is determined with the wall-normal motions, little effect of APG on the wall-normal velocity component results in correspondingly little change in the thermal field (Houra and Nagano, 2006).

The structural differences in quasi-coherent motions reflect on higher-order turbulent statistics, especially third-order moments (Nagano and Tagawa, 1988). The distributions of turbulent transport in the velocity and thermal fields are presented in Fig. 6 (a) and (b), respectively. The definite effects of the APG are clearly seen in the velocity field, i.e., as shown in Fig. 6 (a), the positive region of $-\overline{vuv}$, $\overline{vu^2}$, and $\overline{vv^2}$ in the ZPG flows disappears at the inner region as P^+ increases. Since third-order moments are predominately sensitive to the change of coherent structures such as ejections and sweeps (Nagano and Tagawa, 1988), this result indicates that internal structural changes do occur in the velocity field of APG boundary layers. Negative values of $\overline{vu^2}$ in the near-wall to outer regions demonstrate the existence of turbulent energy transport toward the wall from the regions away from the wall. This important characteristic of the APG flows conforms to our previous result (Nagano *et al.*, 1998; Houra and Nagano, 2006), and is also consistent with the results of Bradshaw (1967), Cutler and Johnston (1989), and Skåre and Krogstad (1994). From Fig. 6 (b), it can be seen that a similar inward transfer takes place in the turbulent transport of the thermal field. However, the change in the thermal field is relatively small compared with that in the velocity field.

Figure 7 shows the instantaneous signal traces of streamwise and wall-normal velocities, $\hat{u}$ and $\hat{v}$, and temperature fluctuations, $\hat{\theta}$, together with the second and third order moments, in the buffer region of the APG flow. The abscissa is the time normalized by the Taylor time scale, τ_E. The normalized period of about ten in the Taylor time scale corresponds to the mean period of the intermittent bursts (Nagano *et al.*, 1998). The circumflex $\hat{}$ denotes the normalization by the respective rms value. The two shaded regions labeled (a) and (b), respectively, correspond to the time periods in Figs. 9 (a) and (b), discussed later.

As seen from Fig. 7, at the time period of (a), the sweep motions ($Q4$: $u > 0$, $v < 0$) largely contribute to the Reynolds shear stress, $-\overline{uv}$, and the wall-normal heat flux, $-\hat{v}\hat{\theta}$. On the contrary, the contributions from the ejection motions ($Q2$: $u < 0$, $v > 0$) are small. Moreover, the $Q2$ motions have small amplitude in the wall-normal velocity and its duration becomes longer. The temperature fluctuations, $\hat{\theta}$, mainly associate with the streamwise velocity fluctuations, $\hat{u}$, and the high correlations, $\hat{u}\hat{\theta}$, are maintained for a long period, as seen at the time period (b). On the other hand, the wall-normal heat flux, $-\hat{v}\hat{\theta}$, occurs intermittently, because it mainly associates with high-frequency $Q4$-motions.

Multi-point measurement results

In order to elucidate the effects of the APG on the dy-

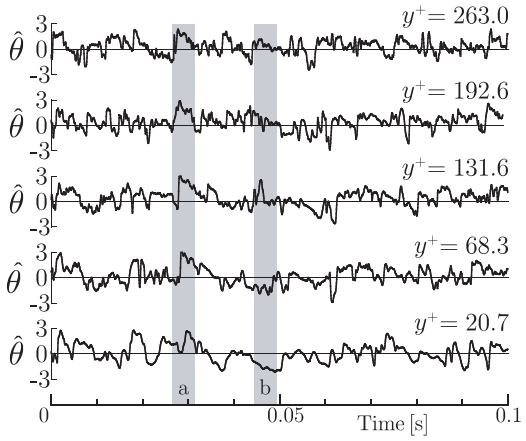

Figure 8: Simultaneously measured temperature signal traces in APG flow ($P^+ = 2.56 \times 10^{-2}$).

namical processes of turbulent transport in the velocity and thermal fields, we have conducted simultaneous measurements with five identical three-wire probes, each of which consists of an X-wire and a fine cold-wire.

Figure 8 shows simultaneously measured temperature signal traces in APG flow. The two shaded regions labeled (a) and (b) respectively correspond to the time periods in Figs. 9 (a) and (b). At the time period (a), a cold region with steep positive gradient followed by mild negative gradient in time occurs over the entire area detected by the probe. This large-scale cold region is caused by the strong sweep motion that frequently observed in APG flow. On the other hand, at the time period (b), locally hot region elongated in time can be seen at the nearest two points from the wall. This high-temperature region near the wall corresponds to the hot-streak as discussed later.

Next, the turbulence fluctuations of the streamwise and wall-normal velocities and temperature can be reasonably interpolated by using the "proper orthogonal decomposition (POD)" based on the eigenfunctions up to the fifth eigenmode (see Houra *et al.*, 2000). The interpolated turbulence statistics showed good agreement with those obtained by a single three-wire probe. The velocity vectors are depicted with respect to an observer's coordinate moving at a speed of about 0.44 $\overline{U}_e$, which is equal to the mean streamwise velocity at $y^+ \simeq 50$ in the APG flow. Figures 9 (a) and (b) show the representative results of velocity vectors and the relevant temperature fluctuations taken at arbitrary times in the APG flow. The vertical axis covers the region from the buffer layer ($y^+ = 20.7$, $y/\delta \simeq 0.04$) to the outside of the log-region ($y^+ = 263.0$, $y/\delta \simeq 0.48$). The abscissa is a time period of 5 ms ($\simeq 4\ \tau_E$ at $y^+ \simeq 50$). The time indications on the abscissa correspond to the shaded regions in Figs. 7, 8, 10 and 11. The solid and broken contour lines represent a hot ($-\theta > 0$) and cold ($-\theta < 0$) region, respectively, and the interval between successive contour lines is $0.05\,\Delta\overline{\Theta}_e$. The shaded regions represent $|\Delta\overline{\Theta}_e| > 0.05$, and the light and dark regions show hot and cold regions, respectively.

As seen from Fig. 9 (a), a large-scale sweep motion ($Q4$) with low temperature becomes dominant, ranging from the inner to the outer regions. These predominating patterns can be categorized in the $Q4$-$Q1$-$Q4$ motion (Nagano and Tagawa, 1995; Houra *et al.*, 2000) corresponding to the high-speed cold region frequently observed in the APG flow. On

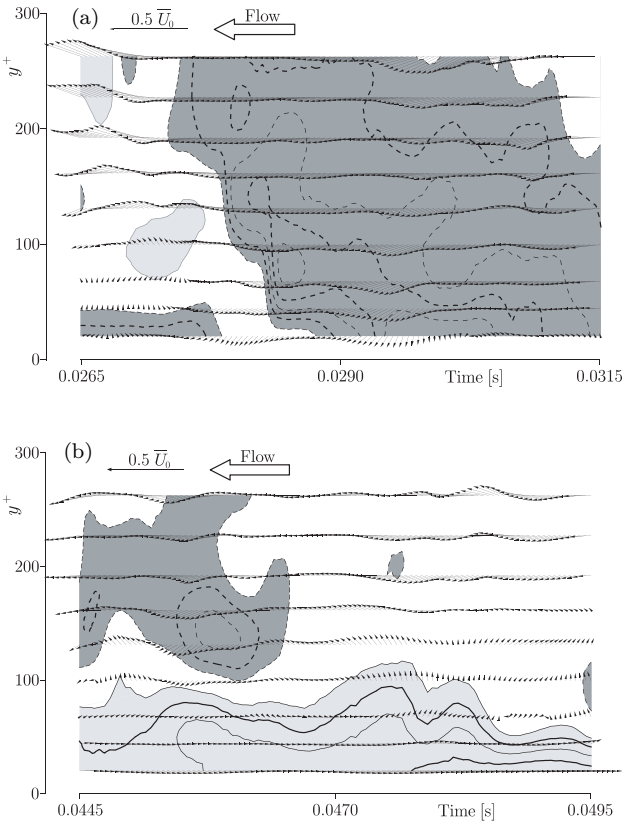

Figure 9: Instantaneous velocity vectors and relevant temperature fluctuations in APG flow: (a) large-scale sweep motion; (b) near-wall elongated hot region. The solid and broken contour lines represent a hot ($-\theta > 0$) and cold ($-\theta < 0$) region, and the interval between successive contour lines is $0.05\,\Delta\overline{\Theta}_e$.

the contrary, Fig. 9 (b) shows the $Q2$-$Q3$-$Q2$ motion associated with an elongated hot region near the wall (i.e., high-temperature low-speed streak). As seen from this figure, the amplitude of the corresponding vectors is relatively small and less active; however, the hot region appears to represent the elongated streaky structure. Thus, the large-amplitude temperature fluctuations are not always associated with strong vertical fluctuations in the APG flow (see the shaded region of (b) in Fig. 7).

Wavelet analysis of multi-point turbulent signals

Finally, to investigate the local relation between the time and scale of the unique turbulence structures that emerged in the APG flow, we analyzed the multi-point signals using the continuous wavelet transform (Nagano and Houra, 2002). The one-dimensional continuous wavelet transform of time-series data $X(t)$ is defined (e.g., Farge *et al.*, 1996; Nagano and Houra, 2002) as:

$$W_X(a,t) = \frac{1}{\sqrt{|a|}} \int_{-\infty}^{\infty} X(t')\,\psi^*\left(\frac{t'-t}{a}\right) dt' \qquad (1)$$

where $\psi(t)$ is an analyzing wavelet, * denotes the complex conjugate, and a is the scaling parameter. As the analyzing wavelet, we adopted the Morlet wavelet,

$$\psi(t) = e^{i2\pi k_\psi t} e^{-t^2/2}, \qquad (2)$$

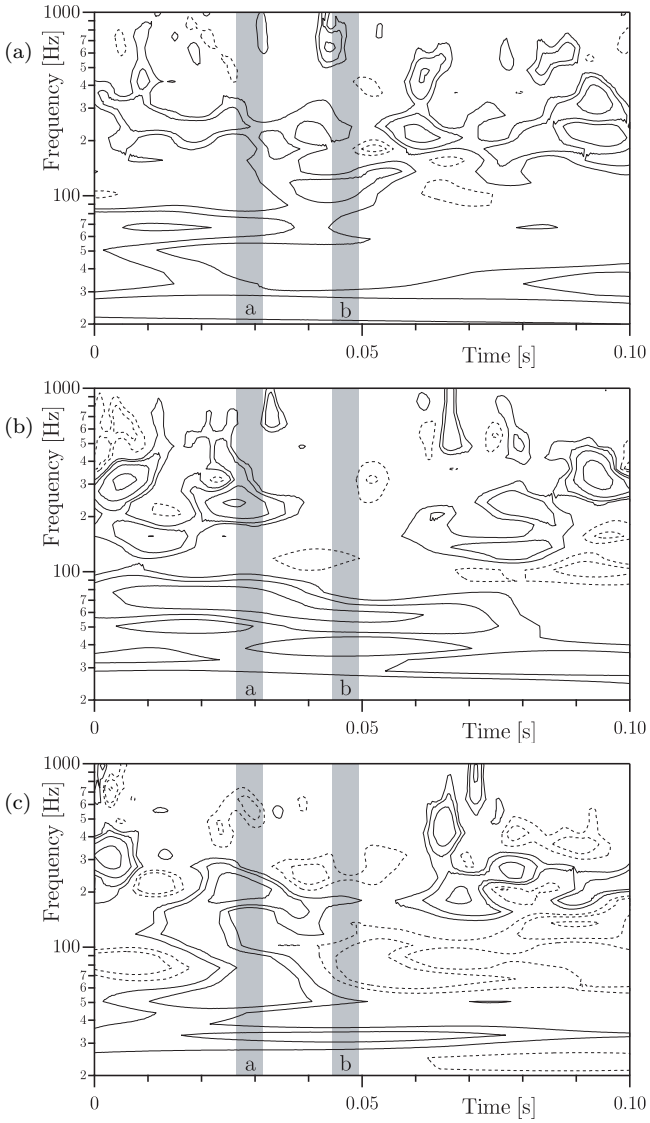

Figure 10: Simultaneously measured wavelet co-scalograms of $-uv$ in APG flow: (a) $y^+ = 131.6$; (b) $y^+ = 68.3$; (c) $y^+ = 20.7$.

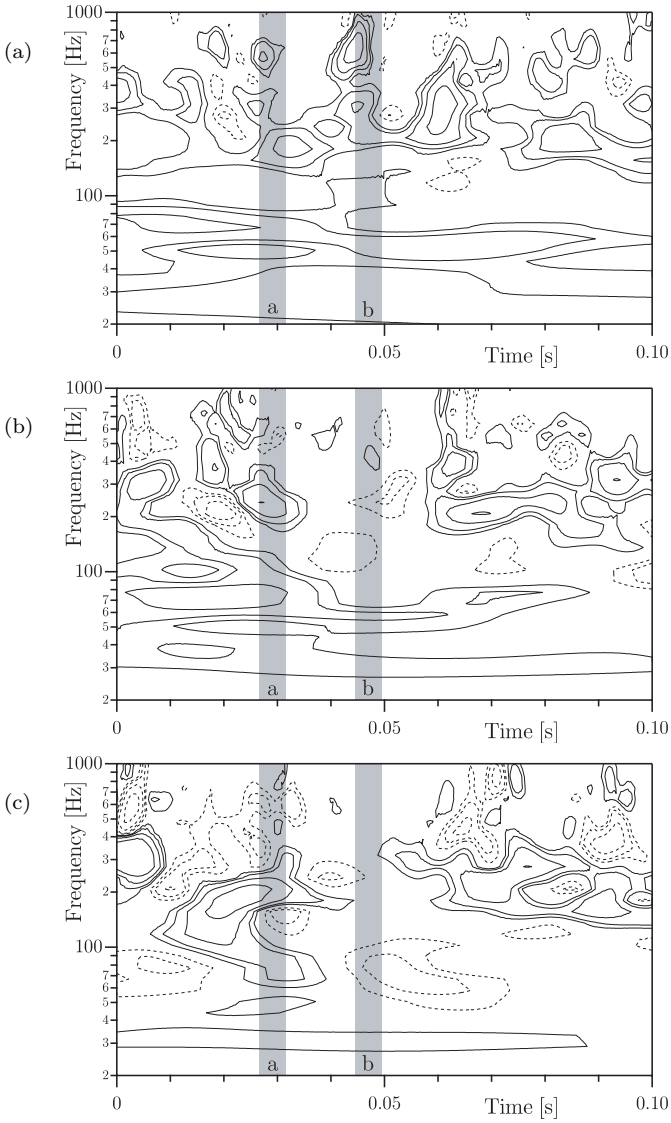

Figure 11: Simultaneously measured wavelet co-scalograms of $-v\theta$ in APG flow: (a) $y^+ = 131.6$; (b) $y^+ = 68.3$; (c) $y^+ = 20.7$.

whose Fourier transform is

$$\hat{\psi}(f) = \sqrt{2\pi}\, e^{-[2\pi(f-k_\psi)]^2/2}. \tag{3}$$

If we put $k_\psi = 1$, the scaling parameter, a, corresponds to the inverse of the frequency as $a = 1/f$. Although the Morlet wavelet does not satisfy the following admissibility condition

$$C_\psi = \int_{-\infty}^{+\infty} \frac{|\hat{\psi}(f)|^2}{|f|}\, df < \infty, \tag{4}$$

we used the empirical approximation and estimated the admissibility constant, C_ψ, for the Morlet wavelet,

$$C_\psi = \int_{-\infty}^{\infty} |\hat{\psi}(f)|^2/|f|\, df \simeq \int_{-\infty}^{\infty} |\hat{\psi}(f)|^2\, df = \sqrt{\pi}. \tag{5}$$

We define the wavelet cross-scalogram as

$$E_{XY}(a,t) = W_X^*(a,t)\, W_Y(a,t). \tag{6}$$

If the analyzing wavelet is complex, the cross-scalogram is also complex and can be written in terms of its real and imaginary parts. The net contribution to the averaged energy is expressed in real values, and we analyze the wavelet co-scalograms, instead of the cross-scalograms.

We take the relation between the second order moment and the wavelet spectrum as

$$\overline{X(t)Y(t)} = \frac{1}{C_\psi} \lim_{T\to\infty} \frac{1}{T} \int_{-\infty}^{\infty} \int_{-T/2}^{T/2} E_{XY}(a,t)\, dt \frac{da}{a^2}. \tag{7}$$

Thus, if we draw the local wavelet spectrum, $(1/a)E_{XY}(a,t)/C_\psi$, onto the scalogram, it corresponds to the Fourier spectrum multiplied by the frequency.

Figs. 10 and 11 respectively show the wavelet co-scalograms of the Reynolds shear stress, $-uv$, and wall-normal heat flux, $-v\theta$, at the nearest three measured points from the wall, i.e., (a) $y^+ = 131.6$, (b) $y^+ = 68.3$ and (c) $y^+ = 20.7$. The solid and broken contour lines represent positive and negative values, respectively. The two shaded regions labeled (a) and (b) respectively correspond to the time periods in Figs. 9 (a) and (b). During the time period (a), the dominating large-scale sweep motions caused the

positive local maximum at about 200 Hz. This corresponds to the energy-containing frequency of the wall-normal velocity fluctuation (not shown here). On the other hand, during the time period (b), there exist only the very low-frequency motions near the wall. However, in the log region ($y^+ = 131.6$), the high-frequency motion (about 600 Hz) has strong energy. This high-frequency motion corresponds to the sweep motions with a cold region above the high-temperature streak as shown in Fig. 9 (b).

CONCLUSIONS

Experimental investigation has been made on a non-equilibrium turbulent boundary layer subjected to adverse-pressure-gradient developing on a uniformly heated flat wall. The spatio-temporal structures educed from a multi-point simultaneous measurement technique are presented. Then, the energy-containing events in the near-wall region are discussed based on the results of the wavelet analysis. From the observation of the instantaneous velocity vectors and temperature fluctuations obtained from the proper orthogonal decomposition (POD), it is found that in the near-wall region, elongated hot regions stay dull and less active; on the other hand, large-scale cold regions having strong energy frequently invade the near-wall region.

ACKNOWLEDGEMENT

This work was partially supported by Grant-in-Aid for Scientific Research (S) (No. 17106003) from the Japan Society for the Promotion of Science (JSPS).

REFERENCES

Blackwell, B. F., Kays, W. M. and Moffat, R. J., 1972, "The Turbulent Boundary Layer on a Porous Plate: An Experimental Study of the Heat Transfer Behavior with Adverse Pressure Gradients," Thermosciences Div., Dept. of Mechanical Engineering, Stanford Univ., HMT-16, Stanford, CA.

Bradshaw, P. and Huang, P. G., 1995, "The Law of the Wall in Turbulent Flow," *Proc. R. Soc. Lond.*,A, **451**, pp. 165–188.

Bradshaw, P., 1967, "The Turbulence Structure of Equilibrium Boundary Layers," *J. Fluid Mech.*, **29**, pp. 625–645.

Cutler, A. D. and Johnston, J. P., 1989, "The Relaxation of a Turbulent Boundary Layer in an Adverse Pressure Gradient," *J. Fluid Mech.*, **200**, pp. 367–387.

Farge, M., Kevlahan, N., Perrier, V. and Goirand, É., 1996, "Wavelets and turbulence," *P*roc of IEEE, **84**, pp. 639–669.

Hishida, M. and Nagano, Y., 1988a "Turbulence Measurements with Symmetrically Bent V-Shaped Hot-Wires. Part 1: Principles of Operation," *Trans. ASME, J. Fluid Engineering*, **110**, pp. 264–269.

Hishida, M. and Nagano, Y., 1988b "Turbulence Measurements with Symmetrically Bent V-Shaped Hot-Wires. Part 2: Measuring Velocity Components and Turbulent Shear Stresses," *Trans. ASME, J. Fluid Engineering*, **110**, pp. 270–274.

Houra, T. and Nagano, Y., 2006, "Effects of Adverse Pressure Gradient on Heat Transfer Mechanism in Thermal Boundary Layer," *Int. J. Heat Fluid Flow*, **27**, pp. 967–976.

Houra, T., Tsuji, T. and Nagano, Y., 2000, "Effects of Adverse Pressure Gradient on Quasi-Coherent Structures in Turbulent Boundary Layer," *Int. J. Heat Fluid Flow*, **21**, pp. 304–311.

Krogstad, P. -Å. and Skåre, P. E., 1995, "Influence of a Strong Adverse Pressure Gradient on the Turbulent Structure in a Boundary Layer," *Phys. Fluids*, **7**, pp. 2014–2024.

Nagano, Y. and Houra, T., 2002, "High-Order Moments and Spectra of Velocity Fluctuations in Adverse-Pressure-Gradient Turbulent Boundary Layer," *Exp. Fluids*, **33**, pp. 22–30.

Nagano, Y. and Tagawa, M., 1988, "Statistical Characteristics of Wall Turbulence with a Passive Scalar," *J. Fluid Mech.*, **196**, pp. 157–185.

Nagano, Y. and Tagawa, M., 1995, "Coherent Motions and Heat Transfer in a Wall Turbulent Shear Flow," *J. Fluid Mech.*, **305**, pp. 127–157.

Nagano, Y., Tsuji, T. and Houra, T., 1998, "Structure of Turbulent Boundary Layer Subjected to Adverse Pressure Gradient," *Int. J. Heat Fluid Flow*, **19**, pp. 563–572.

Skåre, P. E. and Krogstad, P. -Å., 1994, "A Turbulent Equilibrium Boundary Layer near Separation," *J. Fluid Mech.*, **272**, pp. 319–348.

Spalart, P. R., 1988, "Direct Simulation of a Turbulent Boundary Layer up to R_θ=1410," *J. Fluid Mech.*, **187**, pp. 61–98.

Spalart, P. R. and Watmuff, J. H., 1993, "Experimental and Numerical Study of a Turbulent Boundary Layer with Pressure Gradients," *J. Fluid Mech.*, **249**, pp. 337–371.

Verripoulos, C. A., 1983, "Effects of Convex Surface Curvature on Heat Transfer in Turbulent Flow," Ph.D. Thesis, Imperial College.

Volino, R. J. and Simon, T. W., 1997, "Velocity and Temperature Profiles in Turbulent Boundary Layer Flows Experiencing Streamwise Pressure Gradients," *Trans. ASME J. Heat Transfer*, **119**, pp. 433–439.